HAL open science

# Deciphering the role of monosaccharides during phage infection of Staphylococcus aureus

Baptiste Arbez, Marion Gardette, Christophe Gantzer, Neus Vilà, Isabelle Bertrand, Sofiane El-Kirat-Chatel

## To cite this version:

Baptiste Arbez, Marion Gardette, Christophe Gantzer, Neus Vilà, Isabelle Bertrand, et al.. Deciphering the role of monosaccharides during phage infection of Staphylococcus aureus. Nano Research, 2022, 15, pp.9234-9242. 10.1007/s12274-022-4600-3 . hal-03736215

**HAL Id: hal-03736215**

**https://hal.univ-lorraine.fr/hal-03736215v1**

Submitted on 22 Jul 2022

**HAL** is a multi-disciplinary open access archive for the deposit and dissemination of scientific research documents, whether they are published or not. The documents may come from teaching and research institutions in France or abroad, or from public or private research centers.

L'archive ouverte pluridisciplinaire **HAL**, est destinée au dépôt et à la diffusion de documents scientifiques de niveau recherche, publiés ou non, émanant des établissements d'enseignement et de recherche français ou étrangers, des laboratoires publics ou privés.

1 **GRAPHICAL TABLE OF CONTENTS**

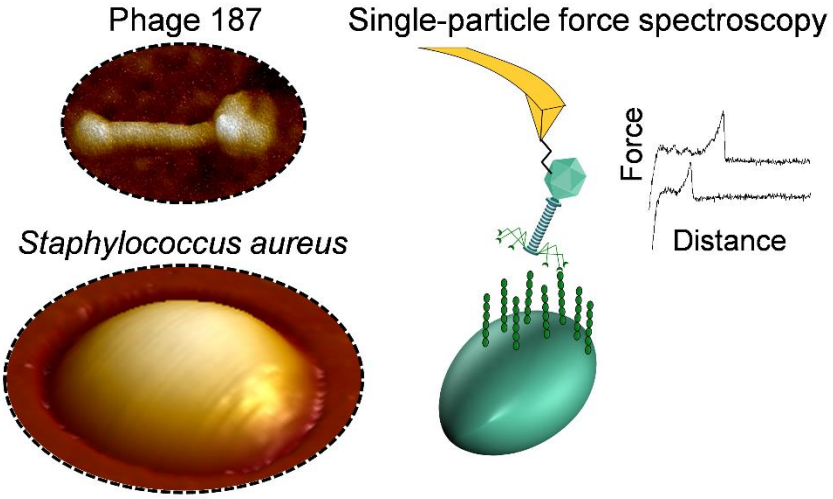


2

3 **Graphical table of contents.** *S. aureus* cell wall was deciphered using a phage-decorated atomic force

4 spectroscopy tip in order to identify major receptors involved in phage adhesion and infection of host cell.

5

# Deciphering the role of monosaccharides during phage infection of *Staphylococcus aureus*.

Baptiste Arbez[a], Marion Gardette[a], Christophe Gantzer[a], Neus Vilà[a], Isabelle Bertrand[a] and Sofiane El-Kirat-Chatel[a]*

[a] Laboratoire de Chimie Physique et Microbiologie pour les Matériaux et l'Environnement (LCPME), CNRS, Université de Lorraine, 405 rue de Vandoeuvre, 54602 Villers-lès-Nancy France

*Address correspondence to Sofiane El-Kirat-Chatel: elkirat1@univ-lorraine.fr

**ABSTRACT**

As phages are extensively investigated as novel therapy tools but also as transfer agents for antibiotic resistance genes, thorough understanding of phage-host interactions becomes crucial. Prerequisite for phage infection is its adhesion to the host surface. Here, we used atomic force microscopy-based single-particle force spectroscopy with phage-decorated tips to decipher the adhesion of phage 187 on living *Staphylococcus aureus* cells. We found that addition of free *N*-acetyl-*D*-glucosamine was able to decrease phage adhesion, suggesting that this monosaccharide plays major role in phage 187 infection of *S. aureus*. Moreover, phage 187 adhesion on monosaccharide-coated model surfaces combined with plaque forming unit counts suggested that a direct link can be established between the propensity to bind to a saccharide and the capability of the latter to inhibit phage infection. On a nanoscale level, single-particle force spectroscopy was successfully used to identify a major receptor required for phage 187 infection of *S. aureus* but also evidenced that this receptor was responsible for phage adhesion on host-cells. Our work demonstrates that single-particle force spectroscopy is a powerful platform to screen and predict the molecular target of phages on their host surfaces.

**KEYWORDS**

Atomic force microscopy, Single-particle force spectroscopy, Phage 187, *S. aureus*, Phage-bacteria interactions

35 **1. INTRODUCTION**

36 Phages are viruses that infect specific bacteria and that can undergo two different life cycles: lysogenic
37 and lytic [1-3]. Lysogenic phages are known to be one of the causes for the increase of multi drug resistance
38 as they promote horizontal gene transfer (HGT) among bacteria [4]. Lytic phages, on the other hand, are
39 suggested to be one of the solutions for the raise of antibiotic-resistant pathogens with phage therapy as
40 they can infect and rapidly kill these pathogens [5-8]. Phages are commercially available as biocontrol
41 agents to help prevent colonization by pathogenic bacteria in agriculture, livestock and food production
42 [9-11], and they present potential applications in wastewater treatment as a method of controlling
43 pathogens in sewage water [12, 13]. After being eclipsed by the use of antibiotics for decades, phages have
44 been regaining attention in the last years due to their implications in the raise of antibiotic-resistant
45 infections and because of their vast potential of applications as antimicrobial agents.

46 All viruses including phages start their infection cycle by non-specific and specific interactions at the
47 surface of their host cells [3, 14]. The recognition of the specific receptor is a key point in the host spectrum
48 of a phage. While very little is known about non-specific interactions, some specific phage receptors are
49 known, but again knowledge remains limited. Recognition is achieved by phage receptor binding proteins
50 (RBPs) and is dependent on location of their target receptors on the bacteria wall surface as well as
51 chemical and structural peculiarities [3, 14-17]. RBPs have strong affinities for specific receptors and allow
52 phages to anchor on their host. Phages have single- or double-stranded DNA or RNA genome surrounded
53 by a capsid. For the vast majority of phages (around 96%), the capsid (or the head) is connected to a protein
54 tail that has RBPs at its other end [18]. Once anchored onto the cell surface, phages can inject their genetic
55 material inside the host cell by using peptidoglycan hydrolases to degrade cell wall locally without lysing
56 the bacteria. Host cells provide the molecular building blocks and enzymes required to replicate phages
57 and produce progeny [1-3].

58 Understanding and characterizing phage-bacteria interactions is critical as they dictate infection [15]. In
59 parallel of genomic and microbiology characterization, physico-chemical characterization of phages gave
60 decisive insights notably through atomic force microscopy (AFM) which contributed intensively in imaging
61 and characterizing the infection process of phages [19-21]. AFM-based force spectroscopy was revealed
62 to be a powerful tool to characterize bacteria interactions with the use of single-molecule force
63 spectroscopy (SMFS) and single-cell force spectroscopy (SCFS) [22-26]. For instance, AFM has already been
64 used to decipher functions of viral attachment proteins in the initiation of infection with reovirus-
65 decorated tips by SMFS on living cells [27]. AFM enables *in situ* characterization of living bacterial cells
66 interactions with phages. However, most studies on living cells focus on the effects of phage infections on
67 bacteria but very few studies focused on phage interactions themselves with single living host-cells to
68 investigate adhesion [21, 28, 29]. In this work, we focus on specific recognition of living *Staphylococcus*
69 *aureus* cells by phage 187 which belongs to the *Siphoviridae* family [30]. *S. aureus*, a Gram-positive
70 bacterium, is a human pathogen of major concerns that can colonize a large variety of tissues in the body
71 [31]. It commonly causes superficial and invasive infections leading to severe morbidity and mortality [32].
72 Treatments of *S. aureus* infections rely on long-term antibiotics which led to the raise of resistant strains
73 such as methicillin-resistant *S. aureus* (MRSA) [33]. In Gram-positive bacteria, lipoteichoic acid (LTA) along
74 with wall teichoic acid (WTA) are two of the major components of the cell envelop and are critical for
75 growth, survival and pathogenicity [34, 35]. LTA and WTA form a polyanionic barrier that is required to
76 maintain metal cation homeostasis and assist in transfers of ions, nutrients and proteins [36-38].
77 Peptidoglicans (PG) in the cell wall form a network on which polymers like WTA, polysaccharides and
78 proteins are covalently linked. *S. aureus* WTA is generally made of repeating units composed of 1,5-D-
79 ribitol-phosphate (RboP) tailored with *D*-alanine esters and mono- or oligosaccharides, commonly *N*-
80 acetyl-*D*-glucosamine (GlcNAc) or *N*-acetyl-*D*-galactosamine (GalNAc) in certain cases [35, 39-41].

81 In the present study, AFM-based single particle force spectroscopy (SPFS) was used to map and probe
82 interactions between single living *S. aureus* cells and phage 187 (Figure 1a). Effects of addition of free
83 monosaccharides on phage infectivity were investigated as well as phage interactions with different
84 monosaccharide-coated model surfaces. Because of *S. aureus* wall composition, GlcNAc and GalNAc were
85 selected as the investigated monosaccharides along with their non-amino homologues: glucose (Glc) and
86 galactose (Gal). This study provided valuable insights into the correlation between the specific ability of
87 phage 187 to adhere on monosaccharide-coated surfaces and the capability of the monosaccharides to
88 inhibit phage infection. On a nanoscale level, SPFS was used to identify a major receptor responsible for
89 phage adhesion on host-cells and thus, a major receptor for phage infection initiation. Our findings helped
90 building a predictive model designed to select best suitable saccharides to reduce phage infectivity by
91 screening saccharide-coated model surfaces with phage-decorated AFM probes. Models developed with
92 SPFS can also be used to predict molecular targets of phages on their host surfaces. This study expands
93 the repertoire of AFM-based force spectroscopy and provides insights into correlation between phage
94 adhesion and infectivity.

95 **2. MATERIALS AND METHODS**

96 **2.1. Bacteria strains and phage 187.**

97 *Staphylococcus aureus* phage 187 (HER 239) and *Staphylococcus aureus* strain 187 (HER 1239) were
98 provided by Félix d'Hérelle Reference Center for Bacterial Viruses from the Université Laval (Québec,
99 Canada). Phages were purified as previously described [42]. Briefly, after replication, phage 187
100 suspensions were centrifugated at 4,000 *g* for 20 min at 4°C and the supernatant was filtered using a 0.45
101 µm membrane (Millex®-GP, Millipore). Then 30 mL of this suspension was concentrated in 10 mL by
102 Amicon Ultra-15 (PLHK, membrane Ultracel-PL, 100 kDa) by centrifugation at 1,000 *g* for 3 min. The phage
103 suspension (2.5 mL) was purified by cesium chloride gradient after addition of 3.88 g CsCl (final volume: 6
104 mL) and centrifugation at 113,000 *g* for 18h at 15°C. About 1.5 mL of phage suspension was extracted from

105 central strip and then purified by dialysis (100 kDa molecular weight cutoff, Spectrum) against phosphate
106 buffered saline (0.1X) for 14 h. The concentration of phages 187 obtained following the above protocol
107 reached $10^9$ PFU/mL. *S. aureus* was routinely grown at 37°C in tryptic soy broth (TSB) media. For phage
108 infection, $10^2$ PFU/mL of phage 187 was incubated with or without free monosaccharides (final
109 concentration 10 mM) in Tris Buffered Saline supplemented with 1 mM $CaCl_2$ and $MgSO_4$ during 2h at room
110 temperature under gentle agitation. *S. aureus* was cultivated in complemented tryptic soy broth to log-
111 phase ($OD_{600}$, approximately 0.2) and infected with equal volume of phage 187. Phages were allowed to
112 absorb for 5 min on *S. aureus* before plating on complemented tryptic soy agar (TSA) for titration.

113 **2.2. Surface and AFM tip functionalization with phages.**

114 Phages were attached covalently on self-assembled monolayers (SAM) of carboxyl-terminated
115 alkanethiols. Briefly, gold substrates and gold coated NPG-D (Bruker) AFM tips were immersed overnight
116 in a solution of 0.1 mM 16-mercaptododecahexanoic acid and 0.9 mM 11-mercapto-1-undecanol to form
117 the SAM. Then, they were washed with ethanol, dried under $N_2$ flow and carboxylic groups were activated
118 by immersion 30 min in a solution of N-hydroxysuccinimide (NHS, 20 mg/mL) and 1-ethyl-3-(3-
119 dimethylaminopropyl)-carbodiimide (EDC, 50 mg/mL). After rinsing with ultrapure water, 2 x $10^8$ PFU of
120 purified phages were added for 1 hour. NHS/EDC coupling formed strong covalent amide bonds between
121 the carboxylic group of the 16-mercaptododecahexanoic acid thiol present on the functionalized gold-
122 coated tips and the amine groups from the phage surface. Finally, surfaces and tips were rinsed in TBS
123 buffer containing 1 mM $CaCl_2$ and $MgSO_4$ ($TBS^+$) and stored for max. 48 h in the same buffer until their use.
124 For AFM images in air, surfaces were gently rinsed in 3 baths of ultrapure water and let to dry overnight
125 at 30°C before imaging.

126 **2.3. AFM imaging and force spectroscopy.**

127 All experiments were achieved at room temperature using a Bioscope Resolve AFM (Bruker corporation,
128 Santa Barbara, CA) and cantilevers spring constants were determined by the thermal noise method [43].

129 Phage immobilized on substrates were imaged in peak-force tapping mode using HIRS-F-B tips in air or in
130 $TBS^+$. For force measurements on cells, stationary phase cultures of *S. aureus* were centrifuged, washed
131 twice in $TBS^+$ and filtered into porous polycarbonate membranes (Millipore). After filtration and rinsing, a
132 1 x 1 $cm^2$ piece of membrane was cut and attached with double sided adhesive tape at the bottom of a
133 Petri dish and immersed in $TBS^+$. First, bare SNL-D tips were used to localize and image individual cells.
134 Then, the tip was replaced by phage decorated tip and adhesion maps of 32 x 32 FD curves on areas of 500
135 x 500 $nm^2$ were recorded on the cell surface with 250 pN applied force, 1 µm/s constant approach and
136 retraction speeds and 250 ms contact time. For inhibition tests, 10 mM of free monosaccharides were
137 added to the Petri dish and adhesion maps were subsequently recorded on the same cells. For force
138 spectroscopy on monosaccharide-coated model surfaces, silicon substrates were immersed overnight in a
139 mixture of 0.9 mM tetraethoxysilane (TEOS, $Si(OCH_2CH_3)_4$), and 0.1 mM isocyanatopropyltriethoxysilane
140 (ICPTES, $(C_2H_5O)_3Si(CH_2)_3NCO$) for silanization and functionalization with isocyanate moieties. Then, they
141 were washed with ethanol, dried under $N_2$ flow and immersed in 10 mM GlcNAc, GalNAc, Glc and Gal for
142 24 hours. Monosaccharide coated substrates were then rinsed with $TBS^+$, imaged in contact mode with
143 bare SNL-D tips and probed with phage decorated NPG-D tips by recording adhesion maps of 5 x 5 $\mu m^2$.

144 **3. RESULTS AND DISCUSSION**

145 3.1. Phage 187 infects S. aureus and can be grafted on gold-coated AFM cantilevers.

146 The first step of this study was to evaluate the infectivity of phage 187 on *S. aureus* by phage plaque assay.
147 Briefly, lysis plaques are clear zones that appear in a homogenous bacteria culture on agar medium due to
148 lysis by phages. Presence of lysis plaques shows the ability of the phage to infect and lyse the bacteria.
149 Lysis plaques are the result of cycles of infection due to one phage (or one aggregate of phages) and
150 occurring cell by cell in all directions from the original infection center thus producing circular areas of lysis
151 called plaque forming unit (PFU) [44]. They represent a simple, cost-efficient and fast technique to

152 evidence and quantify phage infection [45]. When *S. aureus* cells were in contact with purified phages 187,
153 lysis plaques of ~1 mm in diameter were observed (Figure 1b).

154 To probe the interactions between phage 187 and *S. aureus*, we hypothesized that phages can be
155 covalently grafted on gold coated AFM tips using N-hydroxysuccinimide/N-(3-dimethyl-aminopropyl)-N'-
156 ethylcarbodiimide hydrochloride (NHS/EDC) coupling. To confirm this hypothesis, we first functionalized
157 and imaged flat gold substrate. Figure 2 shows topography images of phages covalently attached on gold-
158 coated substrates. Phage 187 is known to have polyhedral shaped heads connected to a tubbed-like tail
159 [46]. In air, the typical shape of S*iphoviridae* was confirmed with the presence of polyhedral heads linked
160 to tails (Figure 2a). Imaging single phage at high resolution revealed a full length of ~200 nm with a head
161 of ~65 nm from the apex to the head-tail joint and a tail length of ~140 nm (Figure 2b). Head height was
162 estimated at ~10 nm and the tail revealed a tubbed-like shape of around 6 nm in height. These
163 morphological features are in good accordance with previous observations of phage 187 achieved by
164 electron microscopy [46]. At the distal end of the tail, an increase of height was observed. We associated
165 it to the baseplate of the phage to which RBPs are attached as already suggested with other phages
166 observed by AFM in the literature [47]. In liquid, the head height was ~25 nm (data not shown). We
167 attributed this height difference to particle collapsing during air drying which is a common phenomenon
168 in AFM phage observations [47]. Remarkably, whereas phage heads were successfully imaged in liquid,
169 tails were not detected or appeared as poorly defined streaks (Figure 2c) probably because they were too
170 flexible or too mobile and were pushed by the scanning tip. As phages were successfully observed in liquid
171 and air, we concluded that phage 187 can be successfully attached to gold substrates. Phages grafted on
172 gold-coated substrate using NHS/EDC coupling led to strong covalent amide bonds that resist forces
173 superior to 2 nN [48, 49]. Therefore, as long as the forces measured by SMFS do not exceed the
174 nanonewton, the amide bond between the phages and the gold-coated AFM tips was considered covalent
175 and irreversible. Thus, we decided to use this approach to functionalize gold-coated AFM tips with phages

176 in order to measure their interaction with living *S. aureus* cell surfaces by mean of AFM-based SPFS (Figure
177 2d).

178 **3.2. Phage 187 recognizes *S. aureus* cell wall with high adhesion frequency.**

179 We probed single living *S. aureus cells* with phage-decorated AFM tips. Figure 3 and S1 show adhesion
180 maps, adhesion force and rupture length histograms as well as representative force-distance (FD) curves
181 obtained by SPFS on live bacteria. For all the cells, adhesion maps did not show cluster patterns, *i.e.*
182 adhesive pixels were randomly spread on the maps (Figure 3a and S1a). This suggested that phage
183 receptors were homogeneously distributed on the host cell surface. Most of the FD curves (51% to 91%
184 depending on the cell) showed adhesive peaks except for cell#S3 (Figure S1b-c) that showed an adhesion
185 frequency of only 17%. Variations in adhesion frequencies between cells were suggested to be caused by
186 slight heterogeneity in cell wall microarchitecture, and composition and/or the angle and position of
187 phage-decorated AFM cantilevers during measurements. Forces mainly ranged from 50 pN to 600 pN
188 (Figure 3b and S1b). This confirmed that phage-bacteria interactions forces were inferior than typical
189 covalent bond forces that exist between the phages and the AFM tips [48]. Thus, we considered that during
190 the repeating approaches and retractions of the AFM tips throughout measurements, weak bonds
191 between phages and cells ruptured before covalent bonds between the phages and the tips. This was
192 further confirmed by the consistent adhesion signatures obtained throughout all the measurements in
193 Figure 3 and S1 and also confirmed with the homogeneousness of the adhesion maps obtained. The
194 majority of rupture lengths ranged between 10 nm and 300 nm (Figure 3c and S1c). Representative FD
195 curves are presented in Figure 3c and S1c as examples. They show the retraction of the AFM tip decorated
196 with the phages. Some curves did not present any adhesion peaks and were considered as “non-adhesive
197 events”. By contrast, adhesive FD curves presented a single or multiple adhesion peaks that we attributed
198 to the interactions between the phage RBPs and the receptors on the cell wall.

199 **3.3. SPFS reveals major cell wall receptors for phage adhesion.**

200 Phage 187 showed homogenous recognition of *S. aureus* cell wall suggesting phage receptors are
201 distributed evenly on the surface of cells. *S. aureus* WTA, which is one of the most abundant components
202 in cell wall, generally presents repeating units composed of RboP with mono- or oligosaccharides residues
203 like GlcNAc or GalNAc [35, 39-41]. We used SPFS to decipher phage interactions with GlcNAc and GalNAc
204 in order to conclude if these monosaccharides lead to specific adhesion of phage 187. Specific adhesion
205 would suggest a probable implication of these molecules in phage recognition process. Interactions with
206 non-amino equivalents, Glc and Gal, were also deciphered. Effect of different monosaccharides on phage
207 infectivity was first investigated at the population scale by incubating phage 187 with free
208 monosaccharides and then quantifying infectivity by PFU counting (Figure 4). When 1 x $10^2$ PFU of phage
209 187 was put in contact with free Glc, Gal, and GalNAc for 2h prior to infection, total phage-infected *S.*
210 *aureus* cells decreased respectively of 22%, 12% and 37% compared to the absence of free
211 monosaccharide. Remarkably, total inhibition was observed with free GlcNAc as no lysis plaques were
212 observed suggesting that no infection occurred or infection was below the detection limit (Figure 4). This
213 suggests that phage 187 RBPs were already saturated with free GlcNAc residues and thus were unable to
214 adsorb and anchor to *S. aureus* cells. Therefore, infection process could not be initiated resulting in a total
215 inhibition of infectivity.

216 To determine the effect of monosaccharides on phage adhesion at the single particle level, living cells were
217 probed with AFM tips decorated with phage 187 in absence or presence of free monosaccharides. As
218 previously discussed, slight quantitative heterogeneity in adhesion frequencies appeared that may be
219 caused by heterogeneities in the cell population. To alleviate this possible undesired parameter and in
220 order to compare the effect of monosaccharides on phage adhesion, the same cell was probed for each
221 measurement before and after monosaccharide addition (Figure 5). *S. aureus* cells were immobilized in
222 porous membranes (Figure 5a). Figure 5b shows the adhesion force histograms obtained without

223 monosaccharide and Figure 5c displays the adhesion force histograms for the same cells with different
224 monosaccharides supplemented in the media. In absence of free monosaccharides, frequencies of
225 adhesive events ranged from 69% to 82% (Figure 5b). When free monosaccharides were added to the
226 media, a decrease in adhesion was observed and frequencies of adhesive events ranged from 25% to 61%
227 (Figure 5c). For all conditions, the number of phage adhesive events on cells decreased but the intensity
228 of interactions, *i.e.* the range of adhesion forces, stayed the same (Figure 5b *vs* 5c). Adhesion frequency
229 decreased from 76% to 42% (*i.e.* a delta of 34%) when free Glc was added in media (Figure 5). With the
230 presence of free GlcNAc, a decrease of adhesion was also observed from 82% to 25% (*i.e.* a delta of 57%).
231 This shows that phage 187 adhesion on *S. aureus* was less prone to happen in presence of free GlcNAc
232 than in presence of free Glc, suggesting that the acetyl amino group of GlcNAc plays a role in phage
233 adhesion and recognition. In presence of free GalNAc, a delta of 33% of adhesive events was observed
234 (from 72% with no GalNAc to 39% with GalNAc). However, the addition of free Gal in the media showed
235 almost no effect on phage adhesion with a variation of adhesion frequency from 69% without Gal to 61%
236 with free Gal (*i.e.* a delta of 8%). Decrease in phage adhesion was more important with free GalNAc
237 compared to free Gal suggesting once again that the acetyl amino group plays a role in phage adhesion
238 and recognition. To confirm these observations, SPFS was repeated on multiple cells. Moreover, the
239 concentration of monosaccharide used is not known to cause any damages to cell walls [50]. But to
240 alleviate any possible contribution of the monosaccharides in the alteration of adhesion signatures and
241 cell integrity, control cells were imaged before and after monosaccharide addition. Addition of
242 monosaccharides did not alter the morphology of bacterial cell wall (Figure S3) thus we assumed that
243 monosaccharides did not cause any damage to the cells that could have altered the adhesion signatures.
244 Figure 6 regroups the results obtained with four cells per monosaccharide tested. GlcNAc induced once
245 more the most important adhesion decrease with a mean delta of 53% ± 4% whereas adhesion decreased
246 by only 15% ± 6% with free Glc. GalNAc and Gal led to a decrease of 24%±6% and 9%±2%, respectively.

247 This confirmed that phage 187 had lessened abilities to adhere on cell wall surface when free GlcNAc,
248 GalNAc or Glc are added in the media and that the acetyl amino groups of GlcNAc and GalNAc play a role
249 on phage adhesion.

250 **3.4. Monosaccharide-coated model surfaces coupled with SPFS can help predict monosaccharide**
251 **effects of phage inhibition.**

252 In order to confirm the specific interaction of phage 187 with different monosaccharides and exclude
253 possible effects of other cell wall components, model surfaces coated with monosaccharides were
254 developed. Model surfaces coated with GlcNAc, GalNAc, Glc and Gal were probed with phage-decorated
255 tip to screen the affinity of phage 187 for each monosaccharide independently (Figure 7a). Topography
256 images of the coated surfaces revealed smooth and homogeneous deposition for all samples with a
257 thickness of ~1.3 nm (Figure 7b). Phage 187 presented high adhesion frequency towards GlcNAc model
258 surfaces (Figure 7c). Adhesion events represented around 93% of the total FD curves for the surface coated
259 with GlcNAc whereas for GalNAc, Gal and Glc, only 32%, 16% and 14% of the FD curves corresponded to
260 adhesive events, respectively. Monosaccharide containing acetyl amino groups led to higher adhesion
261 frequencies than homologous molecules lacking acetyl amino groups. Phage 187 had strongest affinities
262 with these monosaccharides (GlcNAc and GalNAc) which is consistent to the inhibition results of phage
263 187 infectivity in presence of the free monosaccharides. Figure S2 shows three independent SPFS
264 acquisitions on GlcNAc-coated model surfaces. Similarly to acquisitions on cells, adhesion maps on model
265 surfaces revealed an homogeneous distribution of adhesion events (Figure S2a). Adhesion forces ranged
266 from 150 pN to around 700 pN (Figure S2b) which was higher than adhesion forces on cell surfaces. This
267 difference could be explained by a higher density of saccharides on the model surfaces than on the cell
268 wall surface and/or the absence of interferences with other molecules present on the bacteria surface.
269 Rupture lengths however were lower on model surfaces than when SPFS was performed on cells and
270 ranged from 50 to 100 nm (Figure S2c). Molecules grafted on model surfaces were monosaccharides

271 whereas saccharides in *S. aureus* cell wall are mostly in the form of residues in long glycopolymer chains
272 like WTA [35, 39-41]. The difference in the length, and thus in elasticity, between these molecules could
273 explain the lower rupture lengths and the different FD curve signatures observed when monosaccharide-
274 coated model surfaces were scanned by SPFS.

275 Phage-infected *S. aureus* proportion in presence of a monosaccharide was correlated to the adhesion
276 frequency of phage 187 on a model surface coated with the same monosaccharide (Figure 8). In other
277 terms the higher adhesion forces between a monosaccharide (GlcNAc, GalNAc, Glc and Gal) and phage
278 187 are, the better this saccharide will be in inhibiting phage infection. This relationship between adhesion
279 to model surfaces and inhibition of infection can help predict the infectivity of phage 187 on *S. aureus* in
280 presence of a saccharide by screening the adhesion of the phages on a saccharide-coated model surfaces.
281 It would be relevant to test with other saccharides and phages to build a predictive model by extrapolation
282 where screening adhesion forces of a phage with saccharide coated surfaces can help predict the inhibition
283 potential of this saccharide with a specific phage.

284 4. **CONCLUSIONS**

285 With the raise of antibiotic-resistant infections, thorough understanding of phage-host adhesion becomes
286 crucial. This work demonstrates the potential of single-particle force spectroscopy, a homologous
287 technique to single-molecule force spectroscopy and single-cell force spectroscopy, to reveal major cell
288 wall receptors for phages and to help identify best suitable phage infection inhibitors. Phage-decorated
289 atomic force microscopy tips were successfully used to screen phage adhesion on single living cells and on
290 model surfaces coated with molecules of interest. Single-particle force spectroscopy evidenced affinities
291 of phage 187 for monosaccharides presenting acetyl amino groups. It also evidenced that these
292 monosaccharides were able to reduce phage adhesion on *S. aureus* cells after a contact of 2h. Single-
293 particle force spectroscopy combined with plaque forming unit counts showed a direct correlation

294 between phage 187 infectivity in presence of *N*-acetyl-*D*-glucosamine, *N*-acetyl-*D*-galactosamine, glucose
295 and galactose and phage adhesion forces on coated surfaces with these saccharides. This suggested that
296 the higher adhesion forces between a saccharide and phage 187 are, the better this saccharide will be in
297 inhibiting phage infection of *S. aureus*. Single-particle force spectroscopy can help identifying the
298 relationship between the propensity of an inhibitor to bind to phages and the efficacy of inhibition in order
299 to develop models that can predict efficacy of inhibitor only by characterizing phage-inhibitor interactions,
300 for faster inhibitor characterization, and that helps choosing the best suitable inhibitor. This study expands
301 the repertoire of atomic force microscopy-based force spectroscopy and provides insights on correlation
302 between phage adhesion and infectivity.

303 **ACKNOWLEDGEMENTS**

304 We thank the Félix d'Hérelle Reference Center for Bacterial Viruses from the Université Laval (Canada) for
305 providing the phage and the host strain. This work was supported by the Agence Nationale de la Recherche
306 (ANR-20-CE06-0001), the Zone Atelier Moselle (ZAM) and the Lorraine Université d'Excellence (ANR-15-
307 IDEX-04-LUE). We would also like to thank Chloé Retourney and Julie Challant for their help.

308 The authors declare no competing interests.

309 **AUTHOR CONTRIBUTIONS**

310 B.A., M.G., C.G., N.V., I.B. and S.E.K.C designed research; B.A., M.G., N.V. and S.E.K.C performed research;
311 B.A., M.G., C.G., N.V., I.B. and S.E.K.C analyzed data; B.A., M.G., C.G., I.B. and S.E.K.C wrote the original
312 draft.

313 **ELECTRONIC SUPPLEMENTARY MATERIAL (ESM)**

314 Supplementary material (Figure S1 and S2 showing additional adhesion maps recorded on *S. aureus* cells

315 and on GlcNAc-coated model surfaces with AFM tips decorated with phage 187 and Figure S3 showing

316 the impact of GlcNAc on cell wall) is available in the online version of this article.

317

318 **REFERENCES**


319 [1] Clokie, M. R.; Millard, A. D.; Letarov, A. V.; Heaphy, S. Phages in nature. *Bacteriophage* **2011**, *1*,
320 31-45.
321 [2] Doss, J.; Culbertson, K.; Hahn, D.; Camacho, J.; Barekzi, N. A review of phage therapy against
322 bacterial pathogens of aquatic and terrestrial organisms. *Viruses* **2017**, *9*, 50.
323 [3] Dowah, A. S.; Clokie, M. R. Review of the nature, diversity and structure of bacteriophage
324 receptor binding proteins that target Gram-positive bacteria. *Biophys. Rev.* **2018**, *10*, 535-542.
325 [4] Winstel, V.; Liang, C.; Sanchez-Carballo, P.;Steglich, M.; Munar, M.; Bröker, B. M.; Penadés, J.
326 R.;Nübel, U.; Holst, O.; Dandekar, T. Wall teichoic acid structure governs horizontal gene transfer
327 between major bacterial pathogens. *Nat. Commun.* **2013**, *4*, 1-9.
328 [5] Chan, B. K.; Abedon, S. T.; Loc-Carrillo, C. Phage cocktails and the future of phage therapy. *Future*
329 *Microbiol.* **2013**, *8*, 769-783.
330 [6] Moelling, K.; Broecker, F.; Willy, C. A wake-up call: we need phage therapy now. *Viruses* **2018**,
331 *10*, 688.
332 [7] Azam, A. H.; Tanji, Y. Peculiarities of Staphylococcus aureus phages and their possible application
333 in phage therapy. *Appl. Microbiol. Biotechnol.* **2019**, *103*, 4279-4289.
334 [8] Sulakvelidze, A.; Alavidze, Z.; Morris Jr, J. G. Bacteriophage therapy. *Antimicrob. Agents*
335 *Chemother.* **2001**, *45*, 649-659.
336 [9] Jamal, M.; Bukhari, S. M.; Andleeb, S.; Ali, M.; Raza, S.; Nawaz, M. A.; Hussain, T.; Rahman, S. U.;
337 Shah, S. S. Bacteriophages: an overview of the control strategies against multiple bacterial
338 infections in different fields. *J. Basic Microbiol.* **2019**, *59*, 123-133.
339 [10] Sarhan, W. A.; Azzazy, H. M. Phage approved in food, why not as a therapeutic? *Expert Rev Anti*
340 *Infect Ther* **2015**, *13*, 91-101.
341 [11] Żbikowska, K.; Michalczuk, M.; Dolka, B. The use of bacteriophages in the poultry industry.
342 *Animals* **2020**, *10*, 872.
343 [12] Withey, S.; Cartmell, E.; Avery, L.; Stephenson, T. Bacteriophages—potential for application in
344 wastewater treatment processes. *Sci. Total Environ.* **2005**, *339*, 1-18.
345 [13] Periasamy, D.; Sundaram, A. A novel approach for pathogen reduction in wastewater treatment.
346 *J. Environ. Health Sci. Eng.* **2013**, *11*, 1-9.
347 [14] Bertozzi Silva, J.; Storms, Z.; Sauvageau, D. Host receptors for bacteriophage adsorption. *FEMS*
348 *Microbiol. Lett.* **2016**, *363*, fnw002.
349 [15] Stone, E.; Campbell, K.; Grant, I.; McAuliffe, O. Understanding and exploiting phage–host
350 interactions. *Viruses* **2019**, *11*, 567.
351 [16] Rakhuba, D.; Kolomiets, E.; Dey, E. S.; Novik, G. Bacteriophage receptors, mechanisms of phage
352 adsorption and penetration into host cell. *Polish J. Microbiol.* **2010**, *59*, 145.
353 [17] Bielmann, R.; Habann, M.; Eugster, M. R.; Lurz, R.; Calendar, R.; Klumpp, J.; Loessner, M. J.
354 Receptor binding proteins of Listeria monocytogenes bacteriophages A118 and P35 recognize
355 serovar-specific teichoic acids. *Virology* **2015**, *477*, 110-118.
356 [18] Ackermann, H.-W. Bacteriophage observations and evolution. *Res. Microbiol.* **2003**, *154*, 245-
357 251.
358 [19] Dubrovin, E. V.; Voloshin, A. G.; Kraevsky, S. V.; Ignatyuk, T. E.; Abramchuk, S. S.; Yaminsky, I. V.;
359 Ignatov, S. G. Atomic force microscopy investigation of phage infection of bacteria. *Langmuir*
360 **2008**, *24*, 13068-13074.
361 [20] Zago, M.; Scaltriti, E.; Fornasari, M. E.; Rivetti, C.; Grolli, S.; Giraffa, G.; Ramoni, R.; Carminati, D.
362 Epifluorescence and atomic force microscopy: two innovative applications for studying phage–
363 host interactions in Lactobacillus helveticus. *J. Microbiol. Methods* **2012**, *88*, 41-46.

364 [21] Alsteens, D.; Trabelsi, H.; Soumillion, P.; Dufrêne, Y. F. Multiparametric atomic force microscopy
365 imaging of single bacteriophages extruding from living bacteria. *Nat. Commun.* **2013**, *4*, 1-7.
366 [22] Müller, D. J.; Dufrene, Y. F. Atomic force microscopy as a multifunctional molecular toolbox in
367 nanobiotechnology. *Nanosci. Technol.* **2010**, 269-277.
368 [23] Helenius, J.; Heisenberg, C.-P.; Gaub, H. E.; Muller, D. J. Single-cell force spectroscopy. *J. Cell Sci.*
369 **2008**, *121*, 1785-1791.
370 [24] El-Kirat-Chatel, S.; Beaussart, A. Probing bacterial adhesion at the single-molecule and single-cell
371 levels by AFM-based force spectroscopy. In *Nanoscale Imaging*. Springer, 2018; pp 403-414.
372 [25] Beaussart, A.;Feuillie, C.; El-Kirat-Chatel, S. The microbial adhesive arsenal deciphered by atomic
373 force microscopy. *Nanoscale* **2020**, *12*, 23885-23896.
374 [26] Beaussart, A.; El-Kirat-Chatel, S. Microbial adhesion and ultrastructure from the single-molecule
375 to the single-cell levels by Atomic Force Microscopy. *Cell Surf* **2019**, *5*, 100031.
376 [27] Koehler, M.; Aravamudhan, P.; Guzman-Cardozo, C.; Dumitru, A. C.; Yang, J.; Gargiulo,
377 S.;Soumillion, P.; Dermody, T. S.; Alsteens, D. Glycan-mediated enhancement of reovirus
378 receptor binding. *Nat. Commun.* **2019**, *10*, 1-14.
379 [28] Liu, S.; Wang, Y. Application of AFM in microbiology: a review. *Scanning* **2010**, *32*, 61-73.
380 [29] Dubrovin, E. V.; Popova, A. V.; Kraevskiy, S. V.; Ignatov, S. G.; Ignatyuk, T. E.; Yaminsky, I. V.;
381 Volozhantsev, N. V. Atomic Force Microscopy Analysis of the Acinetobacter baumannii
382 Bacteriophage AP22 Lytic Cycle. *PLoS ONE* **2012**, *7*, e47348.
383 [30] Deghorain, M.; Van Melderen, L. The Staphylococci phages family: an overview. *Viruses* **2012**, *4*,
384 3316-3335.
385 [31] Wertheim, H. F.; Melles, D. C.; Vos, M. C.; Van Leeuwen, W.; Van Belkum, A.; Verbrugh, H. A.;
386 Nouwen, J. L. The role of nasal carriage in Staphylococcus aureus infections. *Lancet Infect. Dis.*
387 **2005**, *5*, 751-762.
388 [32] Ford, C. A.; Hurford, I. M.; Cassat, J. E. Antivirulence strategies for the treatment of
389 Staphylococcus aureus infections: a mini review. *Front. Microbiol.* **2021**, *11*, 3568.
390 [33] Lindsay, J. A.; Holden, M. T. Understanding the rise of the superbug: investigation of the
391 evolution and genomic variation of Staphylococcus aureus. *Functional & integrative genomics*
392 **2006**, *6*, 186-201.
393 [34] Seo, H. S.; Cartee, R. T.; Pritchard, D. G.; Nahm, M. H. A new model of pneumococcal lipoteichoic
394 acid structure resolves biochemical, biosynthetic, and serologic inconsistencies of the current
395 model. *J. Bacteriol.* **2008**, *190*, 2379-2387.
396 [35] Brown, S.; Santa Maria Jr, J. P.; Walker, S. Wall teichoic acids of gram-positive bacteria. *Annu.*
397 *Rev. Microbiol.* **2013**, *67*, 313-336.
398 [36] Hughes, A.; Hancock, I.; Baddiley, J. The function of teichoic acids in cation control in bacterial
399 membranes. *Biochem. J.* **1973**, *132*, 83-93.
400 [37] Lambert, P. A.; Hancock, I. C.; Baddiley, J. Occurrence and function of membrane teichoic acids.
401 *Biochim. Biophys. Acta* **1977**, *472*, 1-12.
402 [38] van Wely, K. H.; Swaving, J.; Freudl, R.; Driessen, A. J. Translocation of proteins across the cell
403 envelope of Gram-positive bacteria. *FEMS Microbiol. Rev.* **2001**, *25*, 437-454.
404 [39] Xia, G.; Maier, L.; Sanchez-Carballo, P.; Li, M.; Otto, M.; Holst, O.; Peschel, A. Glycosylation of wall
405 teichoic acid in Staphylococcus aureus by TarM. *J. Biol. Chem.* **2010**, *285*, 13405-13415.
406 [40] Mnich, M. E.; Van Dalen, R.; Gerlach, D.; Hendriks, A.; Xia, G.; Peschel, A.; Van Strijp, J. A.; Van
407 Sorge, N. M. The C-type lectin receptor MGL senses N-acetylgalactosamine on the unique
408 Staphylococcus aureus ST395 wall teichoic acid. *Cell. Microbiol.* **2019**, *21*, e13072.
409 [41] Winstel, V.; Sanchez-Carballo, P.; Holst, O.; Xia, G.; Peschel, A. Biosynthesis of the unique wall
410 teichoic acid of Staphylococcus aureus lineage ST395. *MBio* **2014**, *5*, e00869-00814.

411 [42] Bacharouche, J.; Erdemli, O.; Rivet, R.; Doucoure, B.; Caillet, C.; Mutschler, A.; Lavalle, P.; Duval,
412 J. F. L.; Gantzer, C.; Francius, G. On the Infectivity of Bacteriophages in Polyelectrolyte Multilayer
413 Films: Inhibition or Preservation of Their Bacteriolytic Activity? *ACS Appl Mater Interfaces* **2018**,
414 *10*, 33545-33555.
415 [43] Hutter, J. L.; Bechhoefer, J. Calibration of atomic-force microscope tips. *Review of scientific*
416 *instruments* **1993**, *64*, 1868-1873.
417 [44] You, L.; Yin, J. Amplification and spread of viruses in a growing plaque. *J. Theor. Biol.* **1999**, *200*,
418 365-373.
419 [45] Gallet, R.; Kannoly, S.; Wang, N. Effects of bacteriophage traits on plaque formation. *BMC*
420 *Microbiol.* **2011**, *11*, 1-16.
421 [46] Bradley, D.; Kay, D. The fine structure of bacteriophages. *Microbiology* **1960**, *23*, 553-563.
422 [47] Kuznetsov, Y. G.; Chang, S.-C.; McPherson, A. Investigation of bacteriophage T4 by atomic force
423 microscopy. *Bacteriophage* **2011**, *1*, 165-173.
424 [48] Grandbois, M.; Beyer, M.; Rief, M.; Clausen-Schaumann, H.; Gaub, H. E. How strong is a covalent
425 bond? *Science* **1999**, *283*, 1727-1730.
426 [49] Herman, P.; El-Kirat-Chatel, S.; Beaussart, A.; Geoghegan, J. A.; Foster, T. J.; Dufrêne, Y. F. The
427 binding force of the staphylococcal adhesin SdrG is remarkably strong. *Mol. Microbiol.* **2014**, *93*,
428 356-368.
429 [50] Komatsuzawa, H.; Fujiwara, T.; Nishi, H.; Yamada, S.; Ohara, M.; McCallum, N.; Berger-Bächi, B.;
430 Sugai, M. The gate controlling cell wall synthesis in Staphylococcus aureus. *Mol. Microbiol.* **2004**,
431 *53*, 1221-1231.

432

433 **FIGURES**

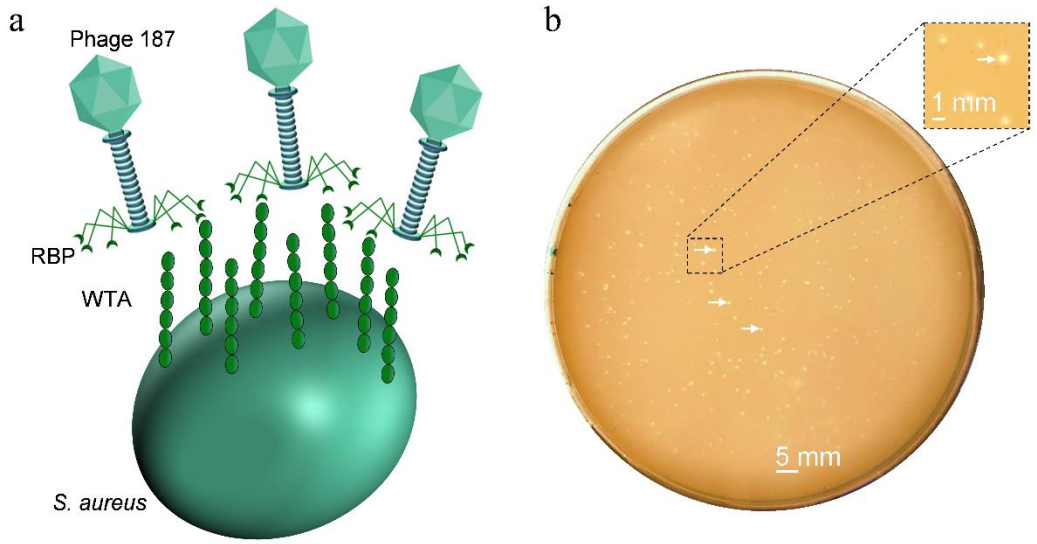


434

435 **Figure 1.** (a) Schematic of the interaction between the phage 187 and *S. aureus.* The phage receptor-
436 binding proteins (RBPs) recognize sub-units of the peptidoglycan-anchored wall teichoic acids (WTA) on *S.*
437 *aureus* surface. (b) PFU obtained after mixing 1 x $10^2$ PFU of purified phage 187 with approximately 1 x $10^8$
438 *S. aureus* cells in TSB medium supplemented with 1 mM $CaCl_2$ and 1 mM $MgSO_4$. A uniform bacterial mat
439 covered the TSA agar in the Petri dish. Bacterial infections lead to lysis plaques (clear dots) of ~1
440 mm diameter where bacteria were lysed and did not grow. For eyes guidance, three lysis plaques
441 are pointed with white arrows and a three-time zoom of a small area is added.

442

443
444

445

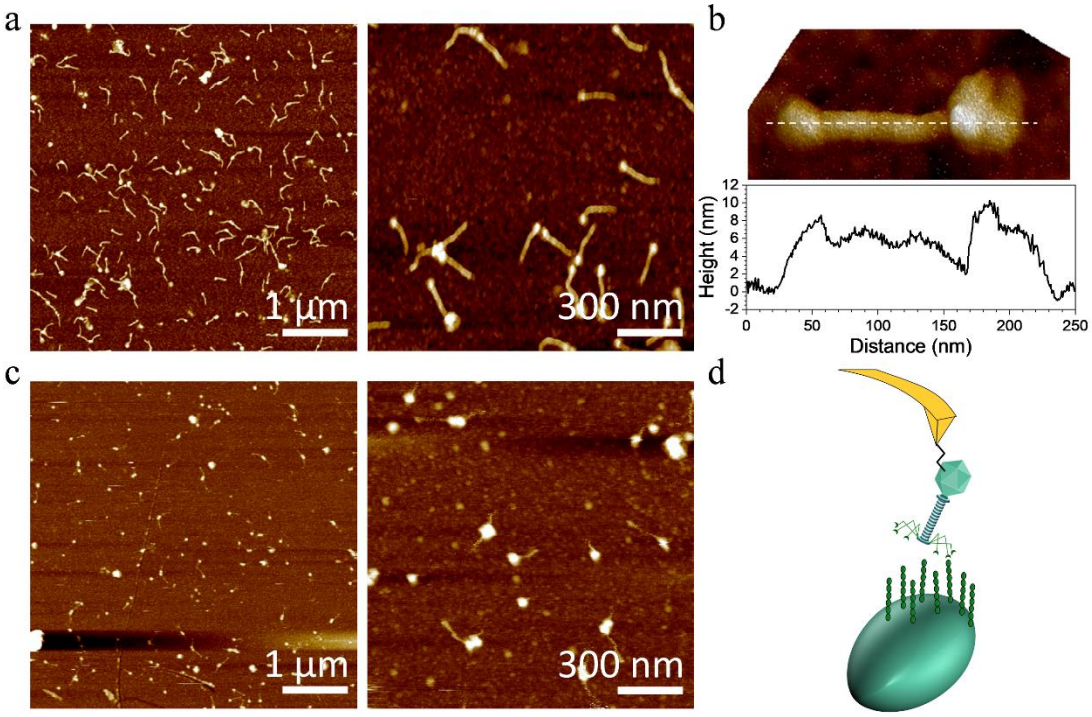


446

447 **Figure 2.** (a) AFM height images in air of purified phage 187 grafted by NHS/EDC coupling on gold-coated
448 surfaces. (b) High resolution topography tridimensional image (500 x 500 nm) in air of a single phage 187
449 covalently immobilized on gold substrate and corresponding cross section taken along the dashed line on
450 the height image. (c) AFM height images in buffer of purified phage 187 grafted by NHS/EDC coupling on
451 gold-coated surfaces. (d) Principle of single particle force spectroscopy where AFM tips decorated with
452 phage 187 are used to probe single *S. aureus* cells.

453

454

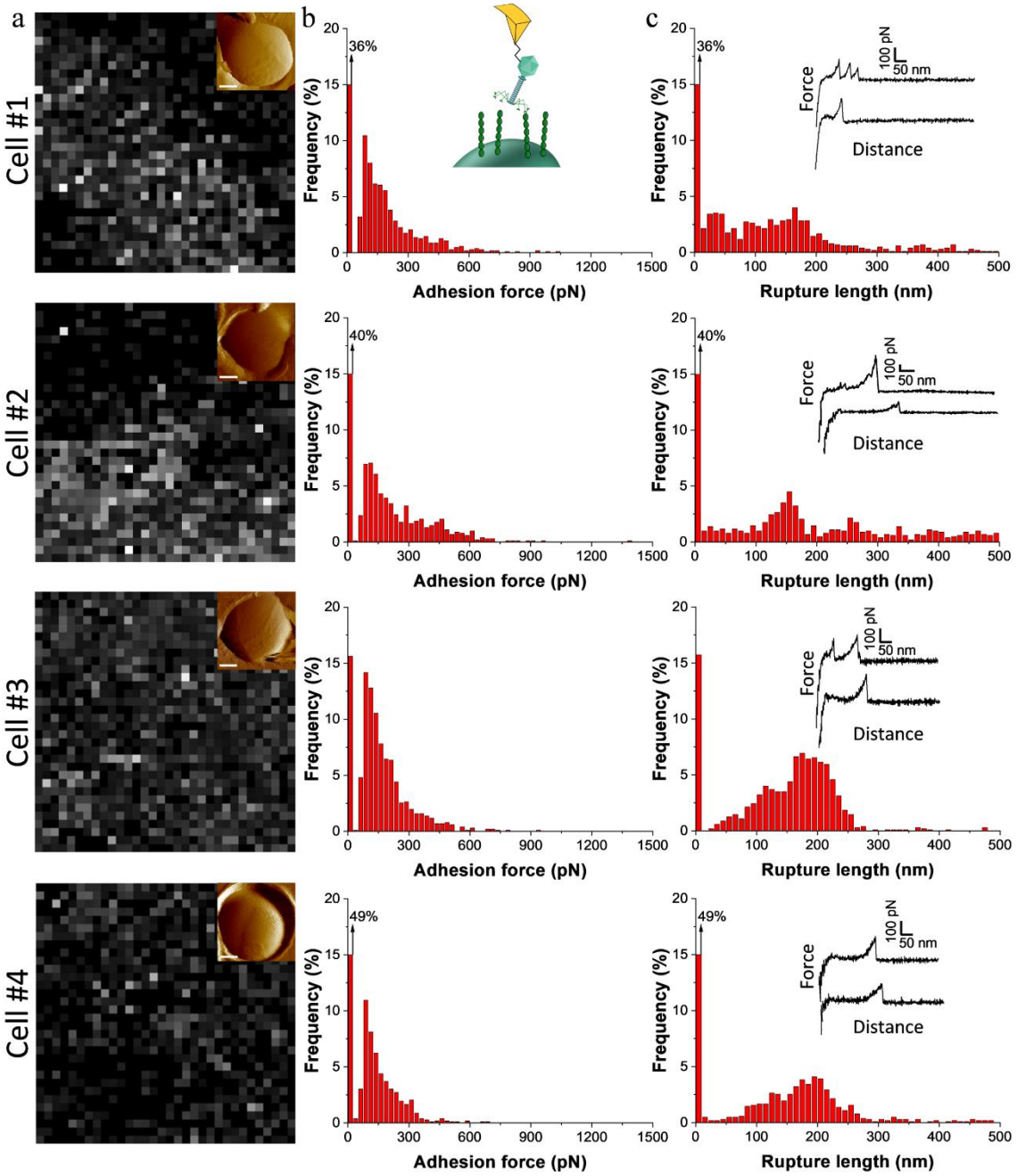


**Figure 3.** (a) Adhesion maps (500 x 500 nm²) recorded on *S. aureus* cells (insets, scale bar = 250 nm) with AFM tips decorated with phage 187. White/grey pixels correspond to adhesive events and black pixels correspond to non-adhesive events (scale 0-1000 pN). (b) Corresponding adhesion force and (c) rupture length histograms together with representative force curves. Data were obtained from three independent experiments using different tips and independent cultures.

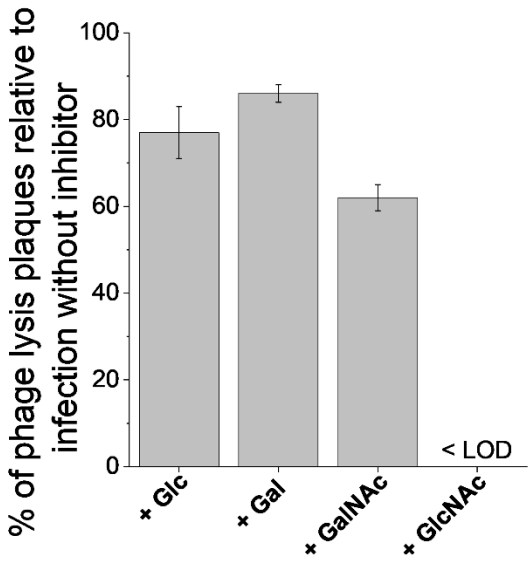


462

463 **Figure 4.** Infectivity of phage 187 towards *S. aureus* cells after 2 hours contact with free monosaccharides

464 (10 mM) determined by plaque forming unit (PFU) counting. *S. aureus* cells (1 x $10^8$) were mixed with

465 phage 187 (1 x $10^2$) and plated on growth media. The percentage of infection was determined by

466 comparison to the number of PFU in absence of free monosaccharides. (Glc: Glucose; Gal: Galactose;

467 GalNAc: N-acetyl-D-galactosamine; GlcNAc: N-acetyl-D-glucosamine; LOD: Limit of detection). Error bars

468 correspond to standard errors calculated from three independent experiments.

469

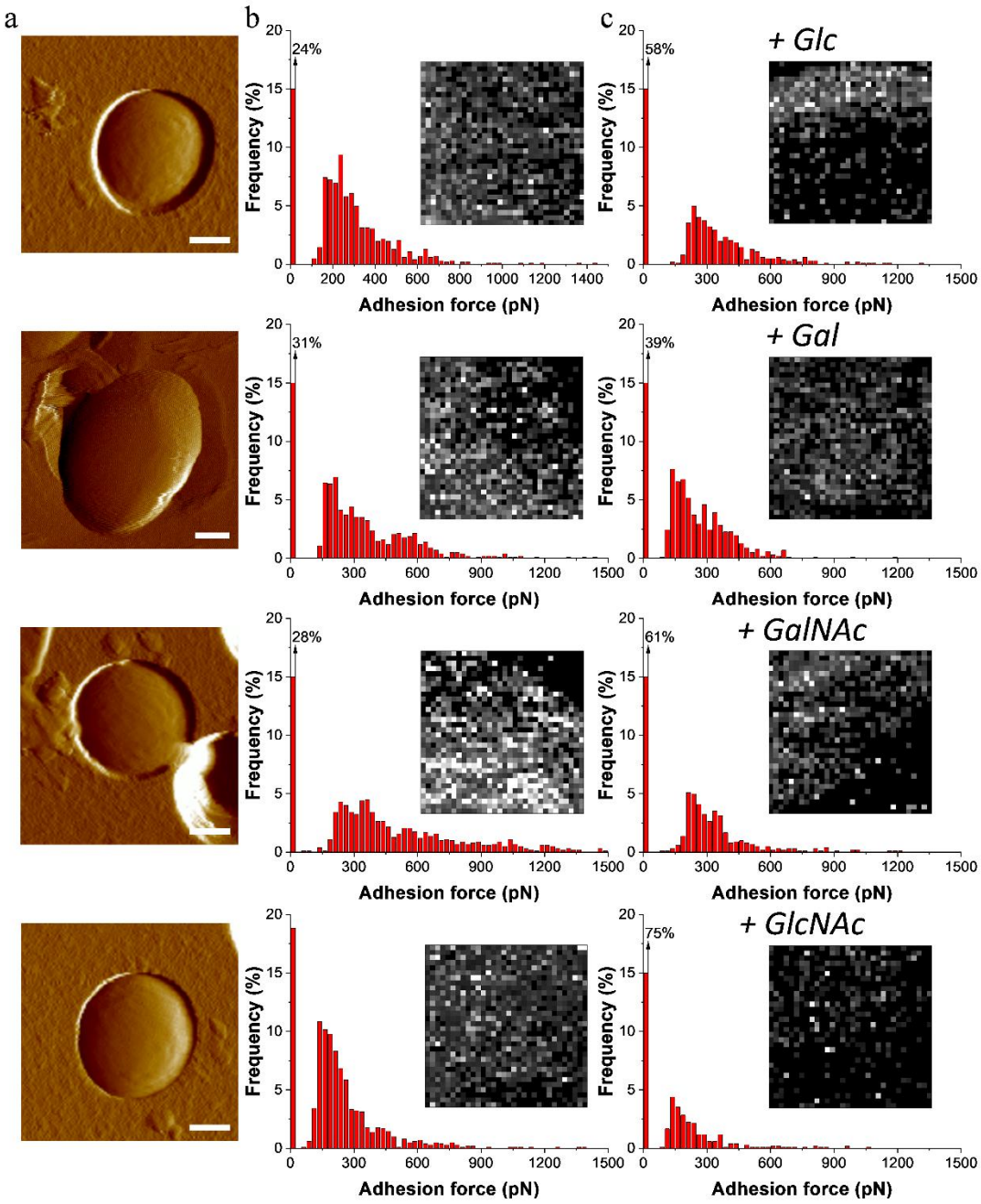


**Figure 5.** (a) Topography images of *S. aureus* cells trapped in porous membranes (scale bar = 250 nm) and probed with AFM tips decorated with phage 187. (b, c) Adhesion force histograms and adhesion force maps (500 x 500 nm², insets) obtained on cells (b) in the absence and (c) in the presence of free monosaccharides (10 mM). White/grey pixels correspond to adhesive events and black pixels correspond

475 to non-adhesive events (scale 0-1000 pN). The added free monosaccharides are indicated above the

476 adhesion force histograms in (c).

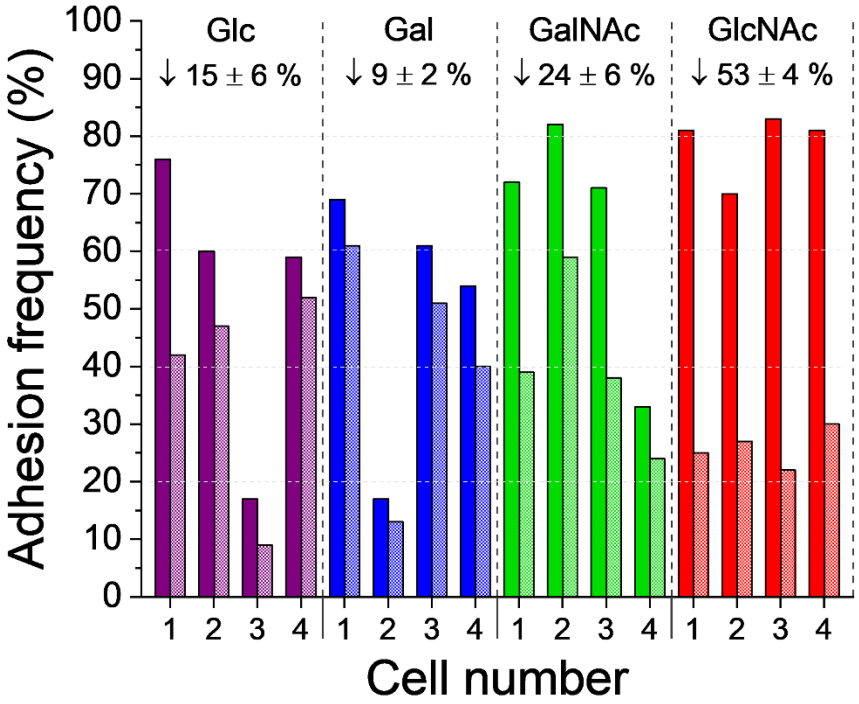


**Figure 6.** Adhesion frequency recorded between the surface of *S. aureus* cells and AFM tips decorated with phage 187 with or without free monosaccharides (10 mM). For each monosaccharide, adhesion maps were recorded on four cells (1-4) in absence (colored bars) or presence (patterned/light colored bars) of free monosaccharides (10 mM) (Purple: Glc; Blue: Gal; Green: GalNAc; Red: GlcNAc). The average decrease is indicated below each monosaccharide name (mean ± s.e.). The adhesion frequency was calculated from the adhesive FD curves obtained among the 1024 FD curves recorded for each map. For each monosaccharide, data were obtained from three independent experiments using different tips and independent cultures.

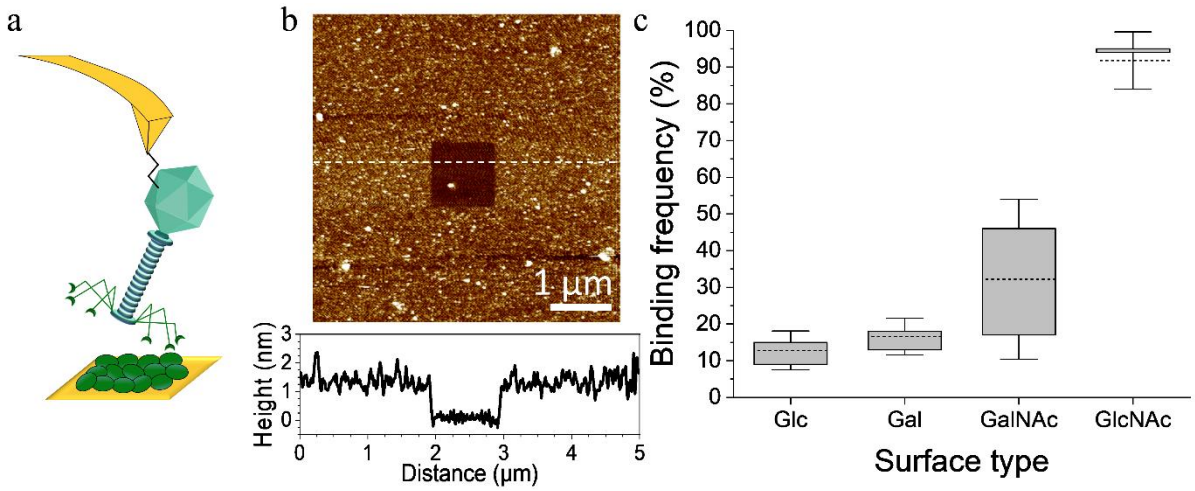


**Figure 7.** (a) AFM tips decorated with phage 187 were used to probe model surfaces coated monosaccharides. (b) Topography (AFM height image; 5 x 5 µm²; z scale = 6 nm) of GlcNAc coated substrates revealing a smooth and homogeneous surface. A vertical cross section taken along the dashed line is shown below the image. The thickness (~1.3 nm) was determined by imaging a square area of 1 x 1 µm² at large forces (>10 nN) before imaging 5 x 5 µm² of the same area at small forces. No scratches were observed for uncoated control surfaces. (c) Boxplot of adhesion frequencies of phage 187-decorated AFM tips on surfaces coated with monosaccharides. Boxes correspond to 25-75 percentiles, dashed lines to means and whiskers to standard deviations. Data were obtained from two independent experiments using different tips and surfaces.

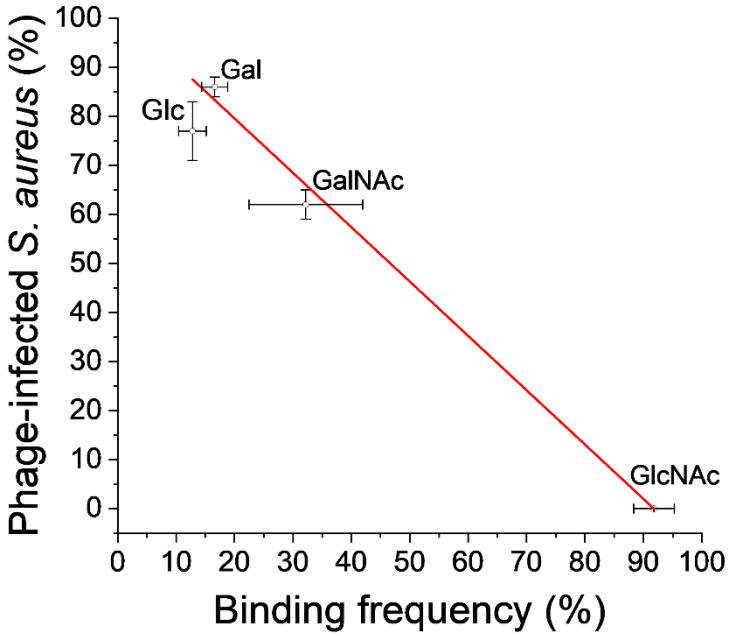


498

499 **Figure 8.** Correlation between the percentage of infected cells in presence of different free

500 monosaccharides and the adhesion frequency of phages towards surfaces coated with monosaccharides

501 (mean ± s.e.). The red line corresponds to a linear fit for eye guidance.

502